High magnetic and super-structural uniformity in fcc supercrystalline films of Co nanoparticles evidenced by MOKE

Caroline Salzemann, Vincent Russier, Matteo Pancaldi, Paolo Vavassori, Andreas Berger, Isabelle Lisiecki

High magnetic and super-structural uniformity in fcc supercrystalline films of Co nanoparticles evidenced by MOKE

Caroline Salzemann[1], Vincent Russier[2], Matteo Pancaldi[3], Paolo Vavassori[4,5], Andreas Berger[4], Isabelle Lisiecki[1*]

1-Sorbonne Université, MONARIS, UMR8233, UMR 8233, F-75005 Paris, France

2- ICMPE UMR 7182 CNRS and Université UPE, 2-8 rue Henri Dunant, 94320 Thiais, France.

3- Department of Molecular Sciences and Nanosystems, Ca' Foscari University of Venice, 30172 Venice, Italy and Elettra-Sincrotrone Trieste S.C.p.A., 34149 Basovizza, Italy

4- CIC nanoGUNE BRTA, E-20018 Donostia-San Sebastián, Spain

5- Ikerbasque, Basque Foundation for Science, E-48013 Bilbao, Spain

Keywords: Supercrystals, Co nanoparticles, MOKE, Monte Carlo simulation, Magnetic and Super-structural uniformity.

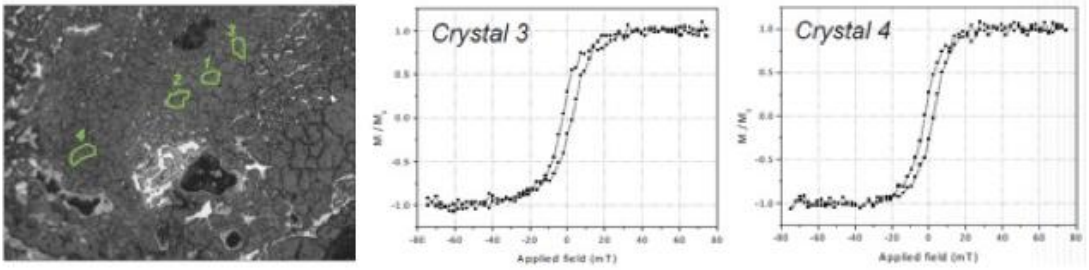

ABSTRACT

In this paper, we report the first local magnetic study, performed by magneto-optical Kerr effect (MOKE), of supercrystals made of magnetic nanoparticles. The supercrystals are characterized by a film morphology and contain several hundred layers of 7.7 nm-Co NPs, ordered in a face-centered cubic (fcc) superstructure. Conversely to the standard superconducting quantum interference device (SQUID)

technique, which provides only a global measurement over an entire sample, the utilization of MOKE enables magnetic measurements of individual localized areas of c.a. 30 μm x 30 μm, from which we can draw conclusions regarding the uniformity of the magnetic properties of the sample, and therefore on the high uniformity of its structure. The latter conclusion is supported by Monte Carlo simulation performed on a model system composed of spherical particles interacting through ~~the~~ dipole-dipole interactions (DDI) and exhibiting a uniaxial magneto-crystalline anisotropy energy (MAE). In addition, by combining these results, with those obtained by SQUID and by grazing incidence small-angle X-ray scattering (GISAXS), we show that magnetic and super-structural properties of supercrystals can be accurately determined.

1. Introduction

3D micrometer-scale self-assemblies of ligand coated nanoparticles (NPs), also called supercrystals, constitutes original nanomaterials [1-4]. These nanomaterials are attractive not only for their applications in many technological domains [5-7] but they also constitute very good models to study crystallization behavior.

Their properties are determined by both those of individual NPs and of their collective interactions. The flexibility of superlattices composition and their superstructures results in a large variety of collective properties including magnetic [8], mechanical [9], transport [5] and vibrational properties [10]. In the case of magnetic supercrystalline films, collective effects depend on various parameters including the dipolar interactions driven by the distance between the NPs and their 3D stacking. When the film extends over the square centimeter scale, structural parameters can vary from one area to another. However, for applications, it is crucial to know if properties are uniform all over the sample (*large scale)*. In addition, the optimization of the performances of these nanomaterials requires a perfect understanding of their properties in relation to their structure at the NP or micrometer scale (*local scale*).

The first reports of nanoparticle superlattices were published by Bentzon and Co. [11,12] in 1989 with iron oxide NPs used as building units. Thereafter, significant progress has been made in preparing 2D and 3D superlattices of magnetic NPs (MNPs). Thin 3D superlattices of MNPs composed of few layers of NPs (3-4 layers) have been obtained for various nanomaterials, such as Co [3,13], FePt [14], FeCoPt [15], Pt_3Ni

[16], and iron oxide [17,18]. By increasing our understanding of the NP assembling process, thicker 3D superlattices, characterized either by a film morphology or isolated (colloidal crystals) have emerged. Hence, supercrystalline films, which can have several tens of layers of NPs have been reported for Co [3, 19], Ni [20], FeCo [21], and iron oxide [22-27] NPs. 3D supercrystal films made from several hundred layers of Co NPs ordered in an fcc superstructure constitute the first reported example of thick magnetic supercrystals [3]. In addition to the film morphology, the growth of isolated magnetic supercrystals, also called colloidal crystals, have been reported in the literature by using Co [4], Fe [28], FePt [29], Pt_3Ni [16] and iron oxide [30-34] NPs. It is noteworthy that the reported studies related to the magnetic supercrystals focused either on the understanding of their growth mechanism, on their structural properties or on their global magnetic properties. To the best of our knowledge, the study of both the local and global magnetic properties combined with a structural characterization of supercrystals by utilizing magneto-optical Kerr effect (MOKE), superconducting quantum interference device (SQUID) and grazing incidence small-angle X-ray scattering (GISAXS) techniques has never been reported.

In this paper, we propose for the first time to locally probe the magnetic properties of supercrystalline films by using the MOKE technique. The supercrystalline films (1 cm x 0.5 cm) studied here contain several hundred layers of dodecanoic acid-coated Co NPs [3], ordered in a face-centered cubic (fcc) superstructure. The MOKE study is performed on various areas of 30 μm x 30 μm, initially selected by scanning electron microscopy (SEM) and optical microscopy. From one area to another, one can see a very good uniformity of the field induced magnetic switching, in terms of the coercivity (H_c), the remanence to saturation magnetization ratio (M_r/M_s) as well the hysteresis loop shape between H_c and its approach towards saturation at higher fields for all temperatures near the ferromagnetic order onset (80 K to 110 K). This behavior, supported by Monte Carlo simulations, which involves two kinds of structures, one well-ordered fcc lattice and another one, namely a hard sphere like disordered structure, highlights a very good super-structural uniformity. Thanks to the combination of the results obtained by using this powerful MOKE technique and those obtained to probe the structural and global magnetic properties by using GISAXS and SQUID respectively, we show that the magnetic and the super-structural properties of supercrystals can be accurately determined, at both local and global length scale.

2. Experimental Section

2.1. Chemical

All materials were used as purchased without further purification. Cobalt acetate and ethanol (VWR), isooctane and hexane (Sigma Aldrich), sodium di(ethylhexyl) sulfosuccinate (Na(AOT)) (Fluka), sodium borohydride and dodecanoic acid (Acros). The synthesis of cobalt(II) bis(2-ethylhexyl)sulfosuccinate, ($Co(AOT)_2$) has been described previously [35].

2.2. Synthesis of dodecanoic acid coated 7.7 nm-Co NPs

Fcc cobalt NPs are synthesized using the micellar approach as described in a previous paper [36]. Dodecanoic acid coating ensures their high stability against coalescence and oxidation. At the end of the synthesis, they are dispersed in hexane. Their mean size and size polydispersity are 7.7 nm and 10 % respectively.

2.3. Synthesis of fcc supercrystalline film of 7.7 nm-Co NPs

3D supercrystalline film is prepared by horizontally immersing a highly oriented pyrolitic graphite (HOPG) substrate (1 x 0.5 cm^2) into a 8 10^{-3} M colloidal solution of Co NPs. Hexane evaporation occurs at 35°C under nitrogen and lasts about 24 h [3].

2.4. Apparatus

- *Transmission Electron Microscopy (TEM)* study is performed using a JEOL JEM-1011 microscope at 100 kV.
- *Scanning Electron Microscopy (SEM)* study is performed using a scanning electron microscope (SEM, JEOL 5510 LV) and a field emission gun scanning electron microscope (FEG-SEM, Hitachi Su-70).
- *Grazing Incidence Small-angle X-ray scattering (GISAXS)* measurements are carried out using a rotating anode generator operated with a small-size focus (copper anode; focus size 0.2 mm x 0.2 mm; 50kV, 30mA). Beam collimation and monochromatization is ensured by a parallel beam multilayer graded mirror optic. The sample is mounted on rotating and translation stages and the diffraction patterns are recorded on photo-stimulable imaging plates. Vacuum pipes are inserted between the sample and the imaging plate to reduce air scattering. During GISAXS measurement the incident beam probes a section ca. 0.8mm in width and extending the sample along.

• To achieve laterally resolved magnetometry, we have utilized Magneto-optical Kerr effect (MOKE) measurements [37].

Specifically, we used a commercial optical wide-field polarization microscope (Zeiss Axio Imager.D1m) optimized for Kerr microscopy (Evico Magnetics GmbH, Germany), for which we had already demonstrated highly sensitive measurements on small sample volumes and sections [38,39].

The microscope is equipped with an electromagnet that allows the application of a magnetic field of up to 500 mT along an arbitrary direction in the sample plane and with a high sensitivity digital CMOS camera (Hamamatsu C11440-42U) that is capable of taking up to 100 images (2048x2048 pixels) per second. The Kerr microscope is equipped with a liquid Nitrogen optical cryostat (temperature range 80-300K) and the sample surface is imaged through a polarization-preserving 50x objective, corrected for the cryostat glass window. Images are processed using the Labview program provided with the microscope (Evico Magnnetics GmbH, Germany). Magnetic-contrast is achieved by inserting and adjusting (rotating) a quarter-wave retarding plate and a polarizer (analyzer) in the reflected light imaging path. Magnetic contrast images of the sample surface with sub-micron spatial resolution are obtained at desired applied magnetic fields by subtracting a background reference image of the sample surface taken at magnetic saturation. The key feature of our approach relies on the fact that the acquisition software allows for measuring a local hysteresis loop, by recoding the magnetic field dependence of light intensity in a selected an arbitrary (shape, size, and position in the field of view) region of interest (ROI) in the image. This corresponds to selecting a reduced number of pixels within the CMOS camera array and use it as a conventional light intensity detector. These pixel arrays are then used as conventional light intensity detectors, which in combination with the polarization optics of the microscope then enable local magneto-optical and associated magnetization measurements as a function of the field. The uncertainties of the determined H_c values is smaller than ± 0.3 mT for all data points, and the uncertainties of the experimentally evaluated M_r/M_s ratios is ± 0.03.

2.5. Monte Carlo simulations

In order to examine the influence of the NP assembly structure on the hysteresis curve characteristics, we have performed Monte Carlo simulations on a model system composed of spherical particles interacting through the dipole-dipole interaction (DDI)

and subjected to an uniaxial magneto-crystalline anisotropy energy (MAE). The simulation box reproduces a film like geometry: it is a parallelepiped box (L_x, L_y L_z) with $L_y = L_z = L$ and $L_x = 0.15L$. The volume fraction is chosen in both cases as $\Phi = 0.45$. Two structures are considered, namely the NP located on the nodes of an ordered FCC lattice and a hard sphere like disordered distribution (HS). In both cases the simulation box includes 600 particles and periodic boundary conditions are used in the (y, z) directions. The MAE coupling constant ($\varepsilon_u = K_1 v/k_B T_0$) is chosen as $\varepsilon_u = 8$ and may represent Co NPs of 7.7 nm (if the reference temperature is taken as $T_0 = 100$K, K_1 is approximately 40 kJ/m3). The DDI coupling constant ε_d is varied in a large range ($\varepsilon_d = \mu_0/4\pi\ (M_s v)^2/d^3/kT_0$ takes a value between c.a. 1.5 for maghemite to c.a. 10 for well crystallized Co). We have considered both low temperature and a temperature not too far from the threshold of the SPM regime, in order to model the experimental results in the 80 K-110 K range.

3. Results and discussion

3.1. Formation of fcc supercrystalline films of Co nanoparticles

Co nanoparticles used to growth the supercrystals are characterized by a mean diameter and size polydispersity of 7.7 nm and 10 % respectively. As shown in the TEM image, (top right inset, Fig. 1), their low size polydispersity favors their spontaneous organization in a 2D hexagonal network in the TEM grid. In addition, thanks to their organic coating

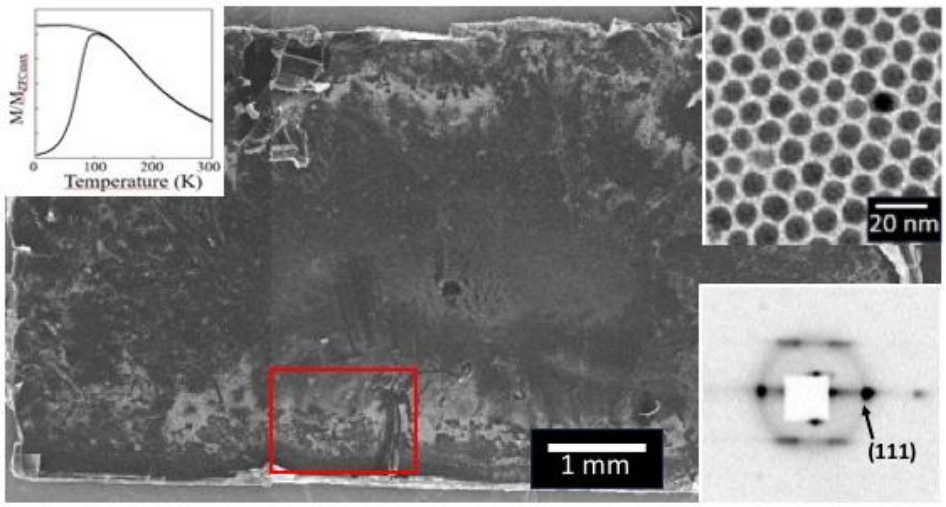

Figure 1. (A) SEM image of supercrystals of 7.7 nm Co nanoparticles deposited on HOPG substrate (10 x 5 mm); (top right inset) TEM image of 7.7 nm Co nanoparticles deposited on copper grid coated with amorphous carbon; (bottom right inset) The X-ray diffraction pattern; (top left inset) Temperature dependence of the magnetization in the zero-field cooled/field cooled (ZFC/FC) curves of supercrystals of Co NPs.

(dodecanoic acid), one can see that they are highly stable against coalescence. The controlled evaporation [3] on HOPG substrate (1 x 0.5 cm^2) of a colloidal solution of 7.7 nm dodecanoic acid coated Co NPs (top right inset, Fig. 1), gives rise to the formation of supercrystalline films. As shown on the scanning electron microscopy (SEM) image (Fig. 1), the deposition appears inhomogeneous, i.e., the film thickness varies from few micrometers on the edge to tens of nanometers in the center of the substrate. The corresponding grazing incidence small-angle X-ray scattering (GISAXS) (bottom right inset, Fig. 1) shows several reflections characteristic of long-range order of the NPs in a fcc superstructure growing in the [111] direction [3]. From the (111) reflection (See arrow), we deduce a stacking periodicity equal to 8.75 nm. This stacking periodicity, $D\sqrt{2}/3$, leads to a coated particle diameter, D, of 10.7 nm including the metal core diameter and a coating contribution (dodecanoic acid chains). Taking into account of the core diameter value, 7.7 nm, this leads to a coating contribution of 1.5 nm, with an interparticle distance (border to border) of 3 nm. This value, which is slightly smaller to the all-trans length of dodecanoic acid, indicates the interdigitation of the alkyl chains, ensuring the structural stability of these supercrystals. The fcc superstructure of these supercrystals and the interparticle distance (border to border), 3 nm found, are in very good agreement with results previously reported for similar supercrystals [4,40,41,42].

3.2. Study of local magnetic properties by MOKE of fcc supercrystalline films of Co nanoparticles

In previous studies, magnetic properties of fcc supercrystalline films similar to the ones studied in this article have been performed several times using either a SQUID magnetometer or a vibrating sample magnetometer (VSM). In these studies, the utilized nanoparticles of cobalt were characterized by similar structural parameters [nanocrystallinity (fcc polycrystals), size (around 7.7±0.4 nm), size distribution (around 10 %) and coating agent (dodecanois acid)]. The supercrystalline films were grown by using the same process as well [4,40,41,42] and the GISAXS measurements did not

indicate any variability in their superstructure, which is always fcc with an interparticle distance of 3 nm. The elaboration of the supercristals is robust and their magnetic properties reported in these prior studies [4,40,41,42] are highly reproducible.

The zero-field cooled (ZFC) and field cooled (FC) magnetization versus temperature curves of fcc supercrystals composed of 8.1±0.4 nm dodecanoic acid-coated Co NPs, are shown on the top left inset of Figure 1 [4]. Measurements have been performed with an applied field of 20 Oe [43]. As the sample has been cooled in zero field, there is no net alignment of the spins at 5 K, and hence the magnetization is close to zero. As the temperature increases, the spins become progressively "unblocked", aligning toward the field direction, and the magnetization increases until it reaches a maximum, which defines the blocking temperature T_B. Above T_B, the behavior is paramagnetic; that is, the thermal energy increases to such an extent that the increased dynamic rotation of the spins prevents alignment along the field direction, and the magnetization decreases with increasing temperature. In the FC curve, the magnetization remains nearly constant from 5 K to T_B at which point the magnetization starts to decrease with increasing temperature in line with the ZFC curve. The supercrystalline sample is characterized by a blocking temperature of around 104 K. The ZFC peak appears narrow, which reflects a narrow distribution of barrier energies, associated with a narrow size distribution of the Co nanoparticles. The flat FC curve at temperatures below T_B is indicative of strong dipolar interactions between the nanocrystals and it has been shown for various similar interacting nanocrystal systems that this is an indication of spin glass-like behavior [44].

In general, SQUID measurements achieve a very high sensitivity. However, these measurements probe the ensemble of the entire sample, giving us only volume averaged information. In order to determine the magnetic homogeneity of our film sample, MOKE microscopy-based magnetometry is performed in this study. Due to its associated short light penetration depth (typically ten to a few tens of nanometers for metallic materials), we can have a surface sensitive characterization. In addition, thanks to the capabilities of our MOKE microscope, one can probe areas of 30 μm x 30 μm or even smaller independently.

The MOKE study is performed on a specifically selected area (see square in Fig. 1). In order to locate this area and accurately identify four small regions to probe their local magnetic properties, prior optical imaging has been done.

Figure 2A shows an optical image at low magnification, were the desired area is identified by means of the superimposed rectangle. By progressively zooming in, four areas of about 30 μm x 30 μm in size and numbered from 1 to 4 are selected (Figs. 2B and 2C and Fig. 3). These four areas have been chosen to have suitable surface structure

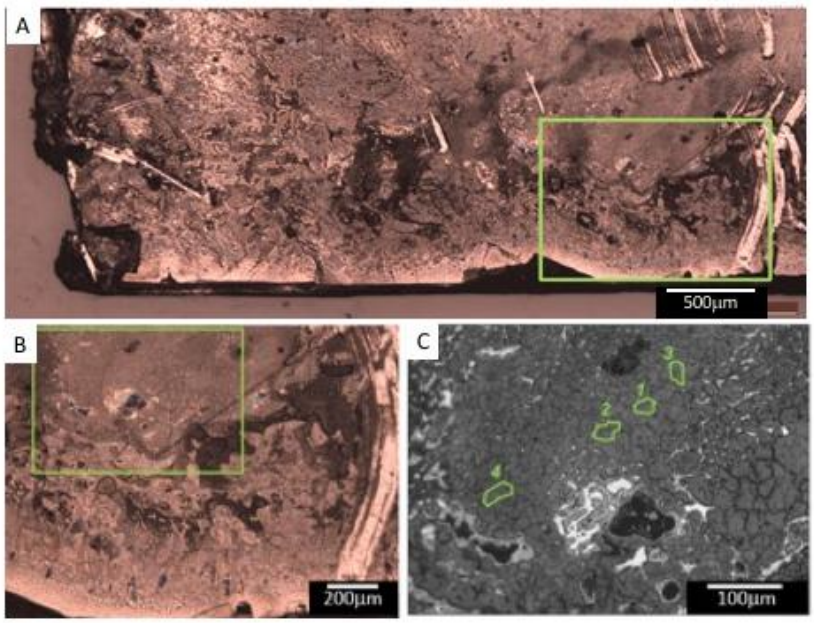

Figure 2. Optical microscopy images of supercrystals of 7.7 nm Co nanoparticles at higher and higher magnifications. These images were taken with the Evico Kerr microscope without utilizing the polarization contrast. (A) shows a broad overview of the sample, identifying the 1st level zoom-in area by a green rectangle. (B) shows the 1st level zoom-in image whose area was identified in (A), and it furthermore defines the 2nd level zoom-in area by means of a green rectangle. (C) shows the 2nd level zoom-in image whose area was identified in (B), and it furthermore defines the 4 local sample areas, for which temperature dependent MOKE data were acquired.

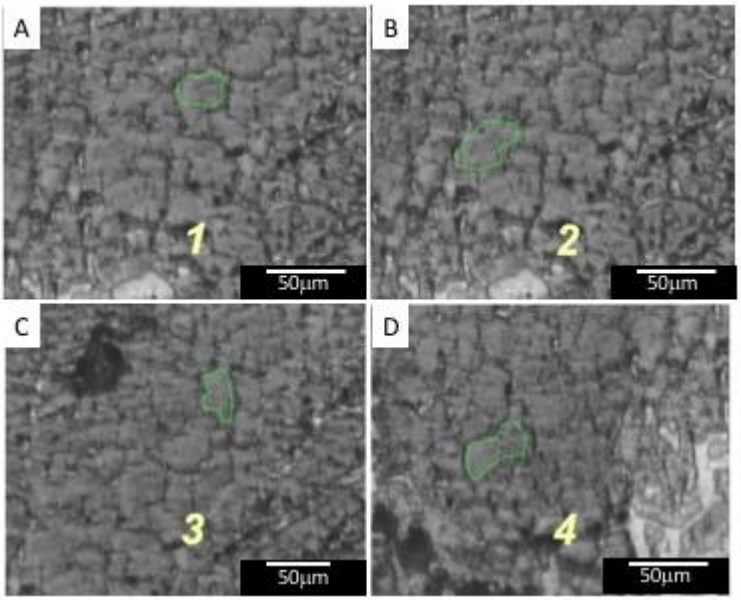

Figure 3. High magnification optical microscopy images of supercrystals of 7.7 nm Co nanoparticles located in the areas 1, 2, 3 and 4 (*see Fig. 2C*) and their immediate surrounding.

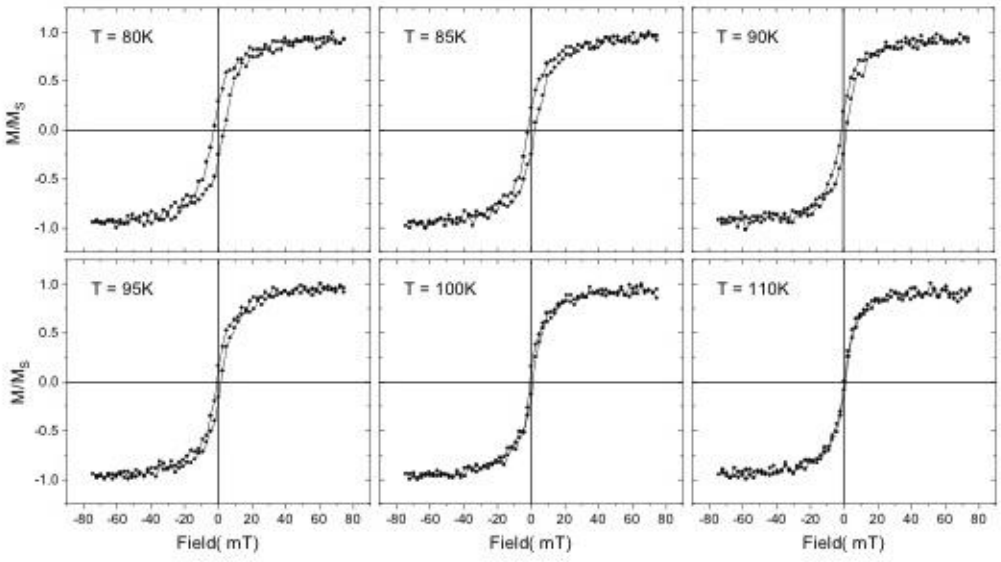

Figure 4. Magnetization versus field curves, from 80K to 110 K, of supercrystal area 1 of 7.7 nm Co nanoparticles (*See Fig. 2C and Fig. 3*). The measurements were done by means of MOKE microscopy and the magnetization values have been normalized to the magneto-optical saturation signal in each measurement.

to perform polarization optics experiments of magnetism without having surface topography polarization effects intermix with MOKE results.

With this approach, hysteresis curves are measured at various temperatures (from 80 K to 110 K) for the four areas independently, (Fig. 4 and Figs. SI.1, SI.2 and SI.3). If we

focus for example on the area numbered 1, and thanks to the very good MOKE signal, we clearly see that the hysteresis loop observed at 80 K gradually becomes thinner and disappears at around 110 K (Fig. 4). By plotting the coercivity H_c in this temperature range, as well as the remanence to saturation magnetization ratio M_r/ M_s, (Figs. 5A, 5B), we observe the strong decay of these two parameters very clearly. This behavior well illustrates the ferromagnetic-to-superparamagnetic transition in the film and allows us to determine the blocking temperature of about around 110K. It is noticeable that this value is in very good agreement with the one found by SQUID measurements in a similar film [4]. This fully validates the use of MOKE in the present study and its complementarity with the SQUID. If we focus on the three other areas (2,3 and 4), very similar behaviors are observed (Fig. SI.1, SI.2, SI.3 (SI) and Figs. 5A, 5B) indicating a very good magnetic transition uniformity from one area to another.

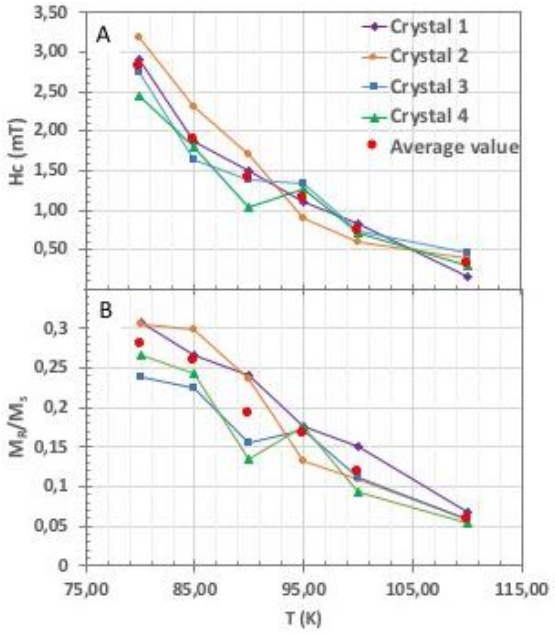

Figure 5. (A) Temperature dependent coercive field, H_c, and (B) remanence to saturation magnetization ratio M_r/M_s (from 80K to 110 K) of supercrystals of 7.7 nm Co nanoparticles located in the areas 1, 2, 3 and 4 (*See Fig. 2C and Fig. 3*). Each individual data point has been extracted from temperature dependent M vs. H measurements that were done locally by means of MOKE microscopy (*See supporting information*).

3.3. Monte Carlo simulation study of the influence of the nanoparticle assembly super-structure on the hysteresis curves.

The results for the coercivity H_c and the remanence to saturation magnetization ratio are shown in Figure 6 and their temperature dependence is given in Figure 7, for $\varepsilon_d = 2$. These

results show an overall agreement with previous simulations [45] while the main difference is the way, in which we introduce the disorder. Notice that for $T^* > 0.6$ both $M_r(T)$ and $H_c(T)$ are in qualitative agreement with the experimental result. We also display in figures 8 and 9, the hysteresis curves at $T^* = 1.0$ and two values of the DDI coupling ($\varepsilon_d = 2, 8$). From these results it is clear that both M_r and H_c depend only weakly on the precise structure (HS or FCC), while conversely the hysteresis shape in the intermediate field range between H_c and the approach of saturation exhibits a significant dependence, especially with the increase of ε_d, on the underlying structural order. Thus, we are led to conclude that the 4 crystals (1 to 4) are likely to correspond to the same super-structural order because of the similitude in their overall hysteresis shape rather than of the close values of M_r and H_c.

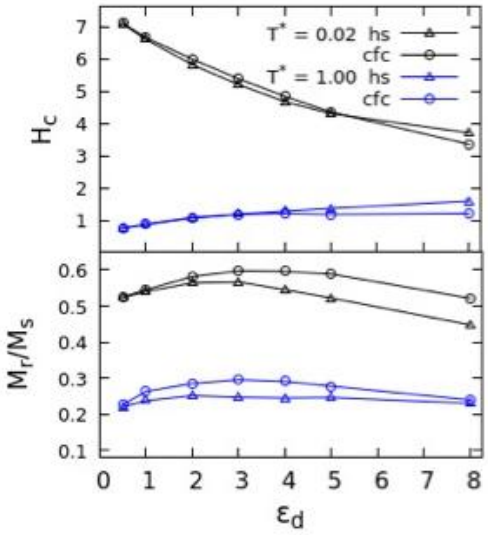

Figure 6. Remanence to saturation magnetization ratio, M_r/M_s and coercive field in reduced unit from Monte Carlo simulations in terms of ε_d for the two structures and two values of the reduced temperature T*.

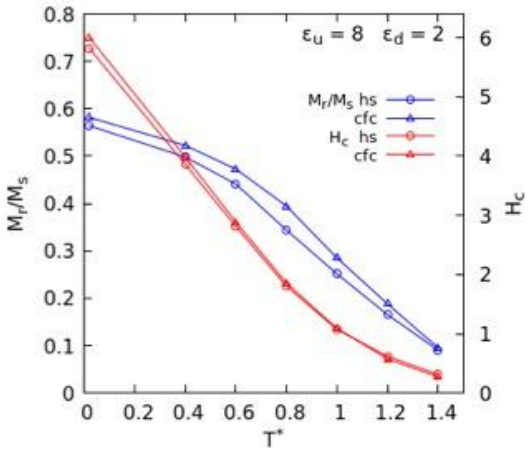

Figure 7. Remanence and coercive field in terms of T^* for the two structures for $\varepsilon_d = 2$.

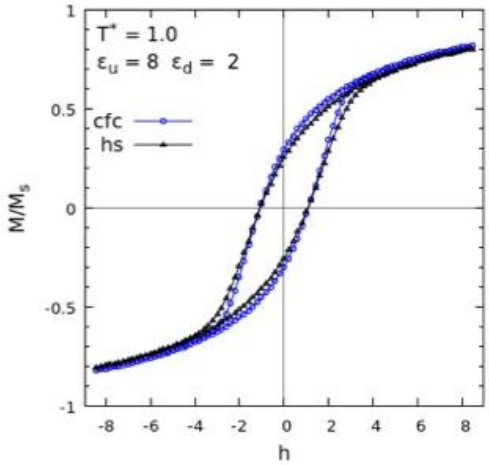

Figure 8. Hysteresis loop simulated by Monte Carlo calculations at a reduced temperature $T^* = 1$ and for the energy coupling constants $\varepsilon_u = 8$ and $\varepsilon_d = 2$ (see text). The reduced field, h, is the applied field in units of $H_r = H_K/2\varepsilon_u$, where H_K is the usual anisotropy field $H_K = 2K/(\mu_0 M_s)$.

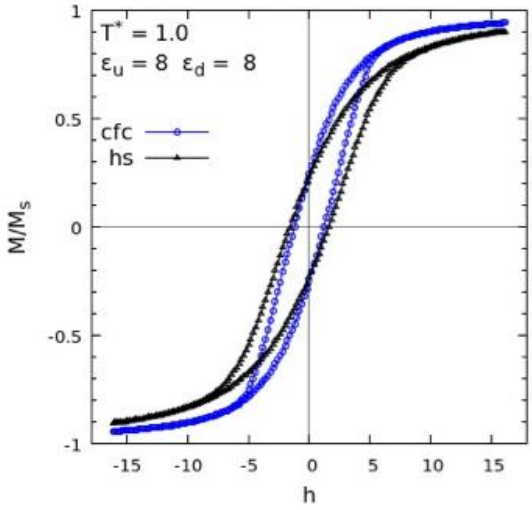

Figure 9. Same as figure 8 for the strongly interacting case, $\varepsilon_d = 8$ and the same anisotropy.

3.4. Complementarity of the global and local techniques (GISAXS, VSM, MOKE) and the Monte Carlo simulation

Thanks to the unique combination of the VSM, the MOKE, the GISAXS techniques and the Monte Carlo simulations proposed in this study, we are able to evidence the high uniformity of the magnetic and structural properties of supercristalline films and to accurately determine them. GISAXS highlights the ordering of the Co NPs in an fcc superstructure with an average interparticle distance (border to border) of 3 nm. VSM, probing the entire sample (centimeter scale), gives average information on the magnetic behavior. The blocking temperature is found around 104 K. In good agreement with the small interparticle distance of 3 nm, strong dipolar interactions between the NPs are observed, which are indicative, in our case, of spin glass-like behavior. MOKE measurements, by probing the sample at the micrometer scale, indicates a high uniformity of the field induced magnetic switching. Independently of the area probed, the blocking temperature is found equal to around 110 K, which is in good agreement with that determines by VSM. In addition, from one area to another, one can also observe invariance in the hysteresis shape in the intermediate field range between the coercive field and the approach of saturation. Monte Carlo simulations clearly evidence that this last feature allows to conclude to the very good uniformity of the fcc super-structural order.

4. Conclusion

In this paper, we highlight the first study of supercrystals of NPs by using Magneto-optical Kerr effect (MOKE) based local magnetometry. Focusing on fcc supercrystals of Co NPs, this study evidences their very good magnetic transition uniformity. Supported by Monte Carlo simulations, our MOKE data allow us to conclude that our sample exhibits a very good magnetic and thus also super-structural uniformity. This unprecedented result, combined to global structural and magnetic properties obtained via GISAXS and SQUID measurements, allows an accurate characterization of supercrystals, including their uniform fcc superstructure as well as uniform superspin glass behavior. These magnetic superlattices provide a new horizon in fundamental physics and are used as model systems for considering phenomena related to dipolar interactions within a solid and in particular dipolar superferromagnetism (SFM),

expected to occur in extremely dense supercrystals. Therefore, their optimal characterization of is crucial importance for further progress in this field.

Acknowledgements :

Authors acknowledge grant access to the HCP resources of CINES under allocation 2022-A0120906180 made by GENCI, CINES, France. Work at nanoGUNE is supported by the Spanish Ministry of Science and Innovation under the Maria de Maeztu Units of Excellence Programme (Grant No. CEX2020-001038-M) and Project No. PID2021-123943NB-I00 (OPTOMETAMAG).

References

[1] K. J. M. Bishop, C. E. Wilmer, S. Soh, B.A. Grzybowski, Nanoscale forces and their uses in self-assembly, Small 5 (2009) 1600–1630.

[2] M. A. Boles, M. Engel, D. V. Talapin, Self-assembly of colloidal nanocrystals: from intricate structures to functional materials, Chem. Rev. 116 (2016) 11220–11289.

[3] I. Lisiecki, P.A. Albouy, M.P. Pileni, Face-centered cubic supracrystals of cobalt nanocrystals, Adv. Mater. 15 (2003) 712-716.

[4] S. Costanzo, A. T. Ngo, V. Russier, P. A. Albouy, G. Simon, Ph. Colomban, C. Salzemann, J. Richardi, I. Lisiecki, Enhanced structural and magnetic properties of fcc colloidal crystals of cobalt nanoparticles, Nanoscale 12 (2020) 24020–24029.

[5] J. Urban, D.V. Talapin, E.V. Shevchenko, C.R. Kagan, C.B. Murray, Synergism in binary nanocrystal superlattices leads to enhanced P-type conductivity in self-assembled PbTe/Ag_2Te thin films, Nat. Mater. 6 (2007) 115-121.

[6] J. Richardi, C. Petit, I. Lisiecki, Magnetic self-organisations of spherical Co nanoparticles used as building blocks: Syntheses, properties and theory. New Trends in Nanoparticle Magnetism. Editors : Dino Fiorani, Davide Peddis et Sara Laureti, (Springer Series in Materials Science) (2021).

[7] J. Park, J. Joo, S. G. Kwon, Y. Jang, T. Hyeon, Synthesis of Monodisperse Spherical Nanocrystals. Angew. Chem. 46 (2007) 4630-4660.

[8] D. Parker, I. Lisiecki, C. Salzemann M.P. Pileni, Emergence of new collective properties of cobalt nanocrystals ordered in fcc supra-crystals: II- magnetic investigation. J. Phys. Chem. C 111 (2007) 12632-12638.

[9] M. Gauvin, N. Yang, E. Barthel, I. Arfaoui, J. Yang, P.A. Albouy, M.P. Pileni, Morphology, nanocrystallinity, and elastic properties of single domain ε Co supracrystals. J. Phys. Chem. C 119 (2015) 7483-7490.

[10] A. Courty, I. Lisiecki, M.P. Pileni, Vibration of self-organized silver nanocrystals. J. Chem. Phys. 116 (2002) 8074-8078.

[11] M. D. Bentzon, J. van Wonterghem, S. Mørup, A. Thölén, C. J. W. Koch, Ordered Aggregates of Ultrafine Iron Oxide Particles: "Super Crystals", Philos. Mag. Part B 60 (1989) 169-178.

[12] M. D. Bentzon, A. R. Thölén, Phase Contrast from a Regular Stacking of Equally Sized Iron-Oxide Spheres, Ultramicroscopy 38 (1991) 105-115.

[13] J.Zhang, Z. Luo, Z. Quan, Y. Wang, A. Kumbhar, D.-M. Smilgies, J. Fang, Low packing density self-assembled superstructure of octahedral Pt_3Ni nanocrystals, Nano Lett. 11 (2011) 2912-2918.

[14] S. Sun,1 C. B. Murray, D. Weller, L. Folks, A. Moser, Monodisperse FePt nanoparticles and ferromagnetic FePt nanocrystal superlattices, Science 287 (2000) 1989-1992.

[15] M. Chen, D. E. Nikles, Synthesis, self-assembly, and magnetic properties of $Fe_xCo_yPt_{100-x-y}$ nanoparticles, Nanoletters 2 (2002) 211-214.

[16] J. Zhang, Z. Luo, Z. Quan, Y. Wang, A. Kumbhar, D.-M. Smilgies, J. Fang, Low packing density self-assembled superstructure of octahedral Pt3Ni nanocrystals, Nano Lett. 11 (2011) 2912-2918.

[17] T. Hyeon, S.S. Lee, J. Park, Y. Chung, H. B. Na, Synthesis of highly crystalline and monodisperse maghemite nanocrystallites without a size-selection process, J. Am. Chem. Soc. 123 (2001) 12798-12801.

[18] S. Sun, H. Zeng, Size-controlled synthesis of magnetite nanoparticles, J. Am. Chem. Soc. 124 (2002) 8204-8205.

[19] F. Dumestre, B. Chaudret, C. Amiens, M. Respaud, P. Fejes, P. Renaud, P. Zurcher, Unprecedented crystalline super-lattices of monodisperse cobalt nanorods, Angew. Chem. Int. Ed. 42 (2003) 5213-5216.

[20] M. Li, Y. Chen, N. Ji, D. Zeng, D.-L. Peng, Preparation of monodisperse Ni nanoparticles and their assembly into 3D nanoparticle superlattices, Materials Chemistry and Physics 147 (2014) 604-610.

[21] C. Desvaux, C. Amiens, P. Fejes, P. Renaud, M. Respaud, P. Lecante, E. Snoeck, B. Chaudret, Multimillimetre-large superlattices of air-stable iron–cobalt nanoparticles, Nature 4 (2005) 750-753.

[22] A. Ahniyaz, Y. Sakamoto, L. Bergstrom, Magnetic field-induced assembly of oriented superlattices from maghemite nanocubes, PNAS 104 (2007) 17570–17574.

[23] E. Josten, E. Wetterskog, A. Glavic, P. Boesecke, A. Feoktystov, E. Brauweiler-Reuters, U. Rücker, G. Salazar-Alvarez, T. Brückel, L. Bergström, Superlattice growth and rearrangement during evaporation-induced nanoparticle self-assembly, Sci. Rep. 7 (2017) 2802-2810.

[24] M. Pauly, B.P. Pichon, P.-A. Albouy, S. Fleutot, C. Leuvrey, M.Trassin, J.-L. Gallania, S. Begin-Colin, Monolayer and multilayer assemblies of spherically and cubic-shaped iron oxide nanoparticles, J. Mater. Chem. 21 (2011) 16018-16027.

[25] H. Yang, T. Ogawa, D. Hasegawa, M. Takahashi, Synthesis and magnetic properties of monodisperse magnetite nanocubes, J. Appl. Phys. 103 (2008) 07D526-1-07D526-3.

[26] L. Zhang, J. Wu, H. Liao, Y. Hou, S. Gao, Octahedral Fe_3O_4 nanoparticles and their assembled structures, Chem. Commun. (2009) 4378-4380.

[27] J. Muro-Cruces, A. G. Roca, A. López-Ortega, E. Fantechi, D. del-Pozo-Bueno, S. Estradé, F. Peiró, B. Sepúlveda, F. Pineider, C. Sangregorio, J. Nogues, Precise size control of the growth of Fe_3O_4 nanocubes over a wide size range using a rationally designed one-pot synthesis, ACS Nano, 13 (2019) 7716-7728.

[28] F. Dumestre, B. Chaudret, C. Amiens, P. Renaud, P. Fejes, Superlattices of iron nanocubes synthesized from $Fe[N(SiMe_3)_2]_2$, Science 303 (2004) 821-823.

[29] E. Shevchenko, D. Talapin, A. Kornowski, F. Wiekhorst, J. Kötzler, M. Haase, A. Rogach, H. Weller, Colloidal crystals of monodisperse FePt nanoparticles grown by a three-layer technique of controlled oversaturation, Adv. Mater. 14 (2002) 287-290.

[30] O. Kasyutich, R. D. Desautels, B. W. Southern, J. van Lierop, Novel aspects of magnetic interactions in a macroscopic 3D nanoparticle-based crystal, Phys. Rev. Lett. 104 (2010) 127205-1-4.

[31] S. Disch, E. Wetterskog, R. P. Hermann, G. Salazar-Alvarez, P. Busch, T. Brückel, L. Bergström, S. Kamali, Shape induced symmetry in self-assembled mesocrystals of iron oxide nanocubes, Nano Lett. 11 (2011) 1651-1656.

[32] L-r Meng, W. Chen, Y. Tan, L. Zou, C. Chen, H. Zhou, Q. Peng, Y. Li, Fe3O4 octahedral colloidal crystals, Nano Res. 4 (2011) 370-375.

[33] E. Wetterskog, M. Agthe, A. Mayence, J. Grins, D. Wang, S. Rana, A. Ahniyaz, G. Salazar-Alvarez, L. Bergström, Precise control over shape and size of iron oxide nanocrystals suitable for assembly into ordered particle arrays, Sci. Technol. Adv. Mater. 15 (2014) 055010-19.

[34] A.-T. Ngo, S. Costanzoa, P.A. Albouy, V. Russier, S. Nakamaed, J. Richardi, I. Lisiecki, Formation of colloidal crystals of maghemite nanoparticles: Experimental and theoretical investigations, Colloids and Surfaces A 560 (2019) 270-277.

[35] C. Petit, P. Lixon, M.P. Pileni, Stuctural study of divalent metal bis(2-ethylexyl) sulfosuccinate aggregates, Langmuir 7 (1991) 2620-2625.

[36] I. Lisiecki, M. P. Pileni, Synthesis of well-defined and low size distribution cobalt nanocrystals: the limited influence of reverse micelles. Langmuir 19 (2003) 9486-9489.

[37] A. Kimel, et al., The 2022 magneto-optics roadmap, J. Phys. D: Appl. Phys. 55 (2022) 463003-463066.

[38] E. Nikulina, O. Idigoras, P. Vavassori, A. Chuvilin, A.; Berger, Magneto-optical magnetometry of individual 30 nm cobalt nanowires grown by electron beam induced deposition, Appl. Phys. Lett. 100 (2012) 100, 142401-142404.

[39] E. Nikulina, O. Idigoras, J.M. Porro, P. Vavassori, A. Chuvilin, A. Berger, Origin and control of magnetic exchange coupling in between focused electron beam deposited cobalt nanostructures, Appl. Phys. Lett. 103 (2013) 123112-123116.

[40] D. Parker, I. Lisiecki, C. Salzemann, M.P. Pileni, Emergence of new collective properties of cobalt nanocrystals ordered in fcc supracrystals: ii, Magnetic investigation, J. Phys. Chem. C 11 (2007) 12632-12638.

[41] D. Polli, I. Lisiecki, H. Portales, G. Cerullo, M.P. Pileni, Low sensitivity of acoustic breathing mode frequency in Co nanocrystals upon change in nanocrystallinity" ACS Nano 5 (2011) 5785-5791.

[42] I. Lisiecki, S. Nakamae, Crystalline order effects on the magnetic properties of superlattices made of cobalt nanocrystals, J. Phys.: Conf. Ser. 521 (2014) 012007-012009.

[43] Magnetic measurements are carried out on a vibrating sample magnetometer (VSM) from Quantum design with a field of 2 mT for the zero-field cooled (ZFC)/field cooled (FC) susceptibility curves. All magnetic measurements are carried out with the applied field parallel to the substrate. In the ZFC measurement, the sample is cooled from 300 K to 3 K with no field and then heated to 300 K in a small field of 2 mT while the magnetization MZFC(T) of the sample is recorded. Then for the FC measurement,

the sample is cooled again to 3 K under the same applied field and the magnetization MFC(T) is recorded.

[44] D. Parker, I. Lisiecki, M. P. Pileni, Do 8 nm Co Nanocrystals in Long-Range-Ordered Face-Centered Cubic (fcc) Supracrystals Show Superspin Glass Behavior? J. Phys. Chem. Lett. 2010, 1, 1139-1142.

[45] D. Kechrakos, K.-N. Trohidou, Magnetic properties of dipolar interacting single-domain particles, Phys. Rev. B 58 (1998) 12169-12177.

SUPPORTING INFORMATIONS

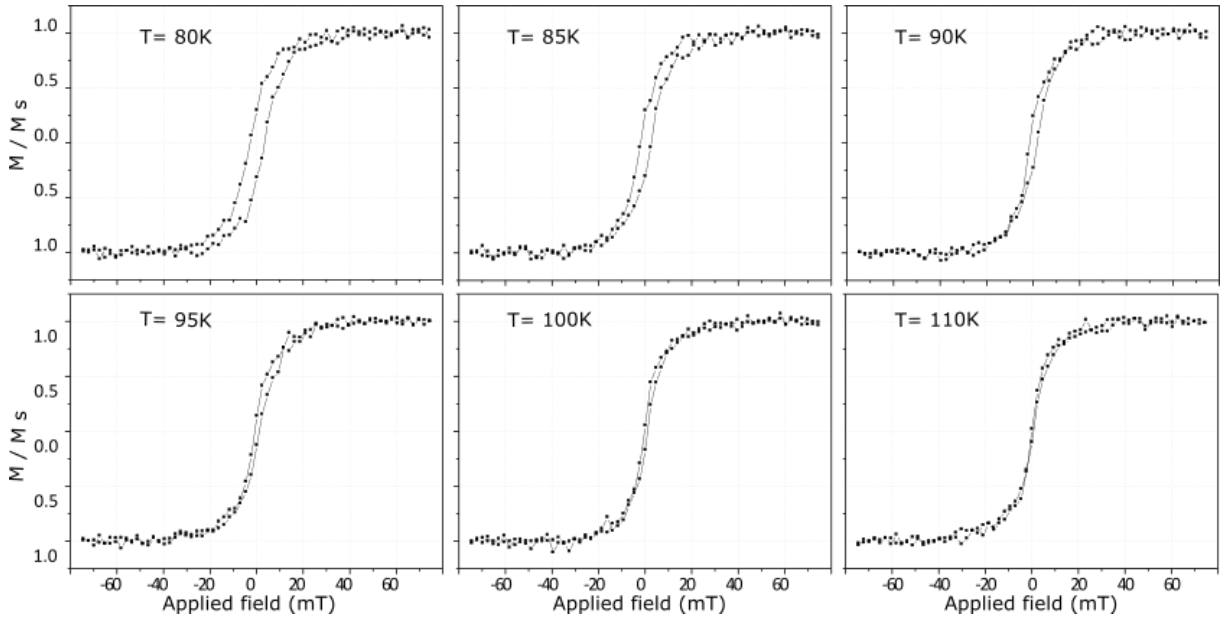

Fig. SI.1 Magnetization versus field curves, from 80K to 110 K, of supercrystal area 2 of 7.7 nm Co nanoparticles (*See Fig. 2C and Fig. 3B*). The measurements were done by means of MOKE microscopy and the magnetization values have been normalized to the magneto-optical saturation signal in each measurement.

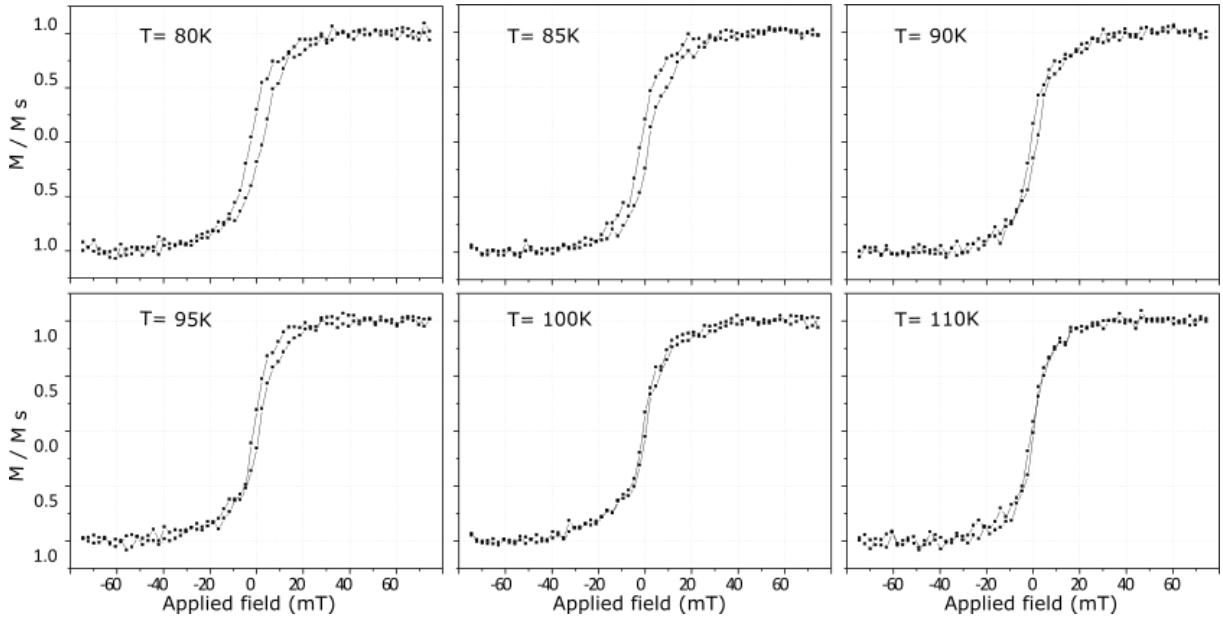

Fig. SI. 2 Magnetization versus field curves, from 80K to 110 K, of supercrystal area 3 of 7.7 nm Co nanoparticles (*See Fig. 2C and Fig. 3C*). The measurements were done by means of MOKE microscopy and the magnetization values have been normalized to the magneto-optical saturation signal in each measurement.

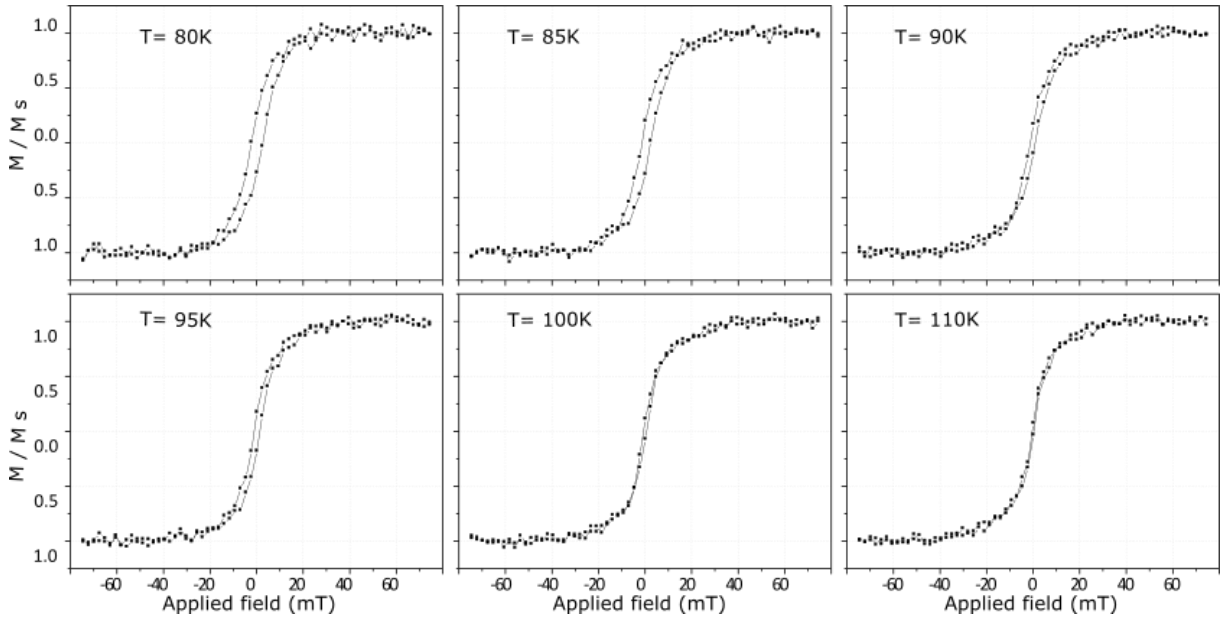

Fig. SI.3 Magnetization versus field curves, from 80K to 110 K, of supercrystal area 4 of 7.7 nm Co nanoparticles (*See Fig. 2C and Fig. 3D*). The measurements were done by means of MOKE microscopy and the magnetization values have been normalized to the magneto-optical saturation signal in each measurement.